NANO LETTERS

2008
Vol. 8, No. 11
3587-3593

Tuning of Vertically-Aligned Carbon Nanotube Diameter and Areal Density through Catalyst Pre-Treatment

Gilbert D. Nessim, A. John Hart,† Jin S. Kim, Donatello Acquaviva,‡ Jihun Oh, Caitlin D. Morgan, Matteo Seita,§ Jeffrey S. Leib, and Carl V. Thompson*

Department of Materials Science and Engineering, Massachusetts Institute of Technology, Cambridge, Massachusetts 02139

Received May 19, 2008; Revised Manuscript Received July 5, 2008

ABSTRACT

By controlling the timing and duration of hydrogen exposure in a fixed thermal process, we tuned the diameters of carbon nanotubes (CNTs) within a vertically aligned film by a factor of 2, and tuned the areal densities by an order of magnitude. The CNT structure is correlated with the catalyst morphology, suggesting that while chemical reduction of the catalyst layer is required for growth, prolonged H_2 exposure not only reduces the iron oxide and enables agglomeration of the Fe film, but also leads to catalyst coarsening. Control of this coarsening process allows tuning of CNT characteristics.

Because of their exceptional and anisotropic properties,[1] layers of aligned carbon nanotubes (CNTs) have been widely investigated for electrical, thermal, and mechanical applications,[2] such as for microelectronic interconnects,[3] heat sinks,[4] and structural composites.[5] These applications require control and optimization of the diameter, wall structure, and areal density of CNTs, particularly in vertically aligned CNT "carpets" grown on and/or transplanted to other substrates.

To replace copper in interlayer vias, some studies suggest using highly packed single-wall CNTs (SWCNTs) to offer the necessary high current-carrying capacity.[6] To match copper conductivity in vias below the 32 nm node, some models[6] suggest a target density of SWCNTs of at least 3.3×10^{13} CNTs/cm^2. Currently achieved maximum densities for CNTs in vias[7] do not exceed 10^{11} CNTs/cm^2. However, other studies show that multiwall CNTs (MWCNTs) with large diameter offer higher than expected conductivity due to the participation of multiple walls to significantly increase the channels for conduction.[8] If interlayer vias are filled with MWCNTs, the target density will be lower than that for SWCNTs, depending of the channels of conduction exhibited by the nanotubes. Furthermore, MWCNTs are usually conducting (statistically, only one third of SWCNTs are conducting).

Process control remains the main obstacle to integration of CNT growth into complex multistep fabrication processes. The CNT growth mechanism is not fully understood and many studies[9−12] have shown very strong sensitivities to small variations in process parameters. CNT growth on a substrate, using thermal chemical vapor deposition (CVD) has two main stages:

(i) Formation and reduction (deoxidation) of catalyst particles.

(ii) Nucleation and growth of the CNTs on catalyst particles.

In many cases, these two stages occur in parallel under fixed processing conditions, obscuring the separate effects of these stages, and making mechanistic understanding and process optimization difficult.

A major challenge is to control the catalyst particle size, as it determines the CNT diameter.[13] Many techniques have been employed to control the catalyst size. For example, controlling the thickness of a metal catalyst thin film has been shown to provide control over the diameter and number of walls of CNTs.[14−16] Additionally, catalyst pretreatment can strongly influence CNT growth. Pretreatment of Fe/Al film in NH_3 at subatmospheric pressure causes restructuring of the catalyst into nanoclusters suitable for low-temperature (350−500 °C) growth of micron-thick carpets of SWCNTs when C_2H_2 is later introduced.[17,18] Alternative techniques for catalyst formation include deposition of preformed metal

* To whom correspondence should be addressed. E-mail: cthomp@mit.edu.
† Department of Mechanical Engineering Massachusetts Institute of Technology, 77 Massachusetts Avenue, Cambridge, Massachusetts 02139. Current address: Department of Mechanical Engineering, University of Michigan, Ann Arbor, MI 48109.
‡ Current address: Laboratory of Micro and Nanoelectronics Devices (LEG2), Ecole Polytechnique, Fédérale de Lausanne (EPFL), Bât ELB 339, Station 11, 1015 Lausanne, Switzerland.
§ Current address: Laboratory for Nanometallurgy, Department of Materials, ETH Zürich, Wolfgang-Pauli-Str. 10, HCI E 522, CH-8093 Zürich, Switzerland.

10.1021/nl801437c CCC: $40.75
Published on Web 10/07/2008

nanoparticles, such as particles templated by block copolymer micelles,[19] which achieve control over the diameter and areal density of CNTs. Additionally, in situ laser ablation of a catalyst target, followed by online sorting using an impactor[7] has been demonstrated to yield catalyst densities of 10^{12}/cm^2 and has yielded CNTs at a density of 10^{11}/cm^2. During CNT nucleation and growth, the challenge is to balance often competing pathways leading to amorphous carbon formation rather than crystalline nanotubes. A common strategy is to add a vapor "etching" agent to the CVD atmosphere, such as H_2, NH_3, O_2, CO_2, or H_2O, or a combination of these agents. In addition to enabling reduction of the catalyst prior to nucleation, H_2 reduces gas-phase pyrolysis of hydrocarbons and also causes desorption of amorphous carbon fragments from the surfaces of catalysts.[13,20] However, hydrogen radicals, which are most abundant in plasma-enhanced CVD atmospheres, can etch small-diameter (particularly small single-wall) CNTs.[21] H_2 used in atmospheric pressure CVD of CNTs using C_2H_4, with a slight addition of H_2O vapor, yields millimeter-thick layers of aligned SWCNTs.[12] In the latter case, it has been proposed that H_2O etches amorphous carbon from the catalysts, thereby increasing the catalyst lifetime.[22] However, the specific conditions that lead to high-yield nucleation[23] and rapid growth of CNTs in this process have not been clearly described in the literature.

In this work, we have analyzed the effects of varying the pretreatment of Fe/Al_2O_3 films in oxidizing (Ar containing parts per million of O_2) and reducing (H_2/Ar) atmospheres during the catalyst preparation stage. While using a defined thermal process, we varied only the timing of the introduction of hydrogen. We find that this leads to tunability of the diameter of CNTs by a factor of 2, and a corresponding increase of the areal density of CNTs by a factor of 10. Further, we found that introduction of H_2 at different times after C_2H_4 was introduced, rather than following the standard practice of simultaneously introducing the reactant and reducing gases, led to significantly enhanced CNT growth rates. We present results from detailed characterization of CNTs grown when varying the time of H_2 introduction relative to the time of C_2H_4 introduction, as well as a detailed analysis of the effects of H_2 on the formation and morphological evolution of the catalyst particles. This is done in order to explain the strong process sensitivity to, and the beneficial effects associated with, control of the sequence and timing of the introduction of reactant and reducing gases.

A film of 1.2/10 nm of Fe/Al_2O_3 was deposited on 150 mm diameter silicon wafers using electron beam evaporation, as described previously.[11] The wafers were manually cleaved into 5 × 5 mm samples using a diamond scribe.

Catalyst pretreatment followed by CNT growth was performed in a three-zone atmospheric-pressure furnace, in a fused-silica tube with an internal diameter of 22 mm. Flows of Ar (99.9995%, Airgas), C_2H_4 (99.5%, Airgas), and H_2 (99.999%, Airgas) were maintained using electronic mass flow controllers (MKS, model 1179A). The substrate sample was held in the tube using a custom-made quartz fixture, and faced the flow at an inclination of 20°.

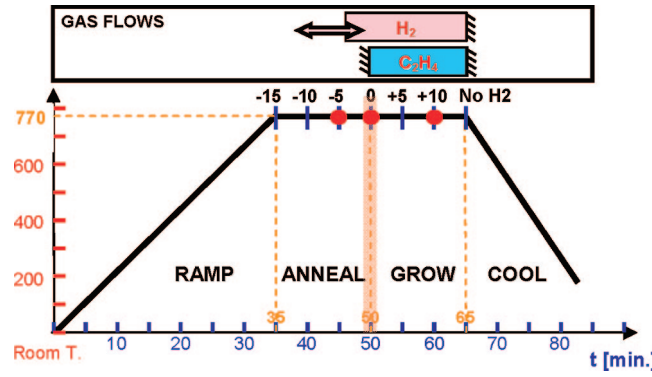

Figure 1. Thermal schedule used for CVD growth of CNTs, where the only variable is the timing of H_2 introduction relative to the time of introduction of C_2H_4. Argon is the carrier gas and has a flow rate of 600 sccm when hydrogen is not present and 200 sccm when mixed with hydrogen. The red dots indicate experimental conditions for which CNTs were characterized using HRTEM.

After flushing the tube with Ar for 10 min, the furnace was ramped to 770 °C over 35 min and the temperature was then held at 770 °C for 30 min, during which C_2H_4 was introduced after 15 min and H_2 was introduced at different times in different runs. Ar continuously flowed through the system during the heating, annealing, growth, and cooling stages. The argon flow rate was 600 standard cubic centimeters per minute (sccm) when H_2 was not present and 200 sccm when H_2 was added. The flow rate of C_2H_4 was 150 sccm and the flow rate of H_2 was 400 sccm. The time/temperature/flow sequence is illustrated in Figure 1. We identify the first 15 min at 770 °C as the "annealing" phase. At the end of this phase, the C_2H_4 was introduced, so that the subsequent 15 min at 770 °C will be referred to as the "growth" phase. H_2 was introduced either before, simultaneously with, or after introduction of the C_2H_4. We will use the following notation to indicate the time of introduction of the H_2: H_2@−5 will indicate that H_2 was introduced at t = 45 min (45 min after the experiment was started at room temperature), which is 10 min after the beginning of the annealing phase and 5 min before the introduction of C_2H_4, which always occurred at the beginning of the growth stage (t = 50 min.).

The CNTs were examined using scanning electron microscopy (SEM, Philips XL-30) and high-resolution transmission electron microscopy (HRTEM, JEOL 2011). The areal density of the CNTs within a film was determined using the mass of an average CNT (based on the inner and outer diameters determined from approximately 50 CNTs measured from each sample using HRTEM), the film volume (which is estimated using SEM imaging), and the film mass, as measured using a microbalance (Sartorius ME36S). The substrate morphology was characterized using atomic force microscopy (AFM, Veeco Nanoscope IV) in tapping mode.

When we introduced hydrogen at any time between H_2@−10 (t = 40 min) and H_2@+10 (t = 60 min), we obtained vertically aligned "carpets" of multiwall CNTs with thicknesses (average tube lengths) of several hundred microns. However, changes in the timing of H_2 introduction relative to the time of C_2H_4 introduction led to significant

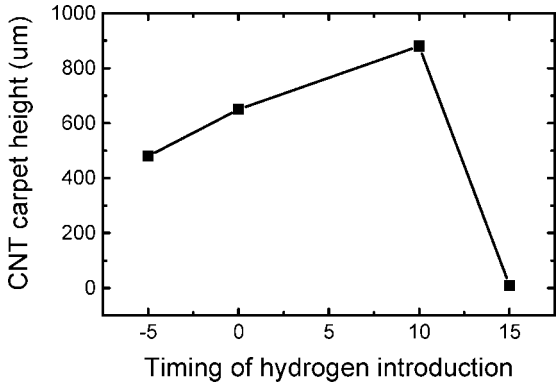

Figure 2. CNT carpet height, as measured using an SEM, as a function of the time of hydrogen introduction relative to the time of ethylene introduction for the process described in the text and Figure 1.

Table 1. Measurements of CNTs from the Three Processes Indicated by the Red Dots in Figure 1[a]

CNT characteristics for different durations of H_2 exposure, relative to the time of C_2H_4 introduction			
	H_2@−5	H_2@0	H_2@+10
outer diameter [nm]	13.6 ± 1.9	9.8 ± 1.8	7.4 ± 1.0
inner diameter [nm]	8.6 ± 1.7	6.6 ± 1.7	5.3 ± 0.9
number of walls	7.3 ± 1.1	4.7 ± 1.0	3.0 ± 0.9
CNT areal density [cm^2]	3.9×10^9	2.6×10^{10}	4.9×10^{10}
CNT carpet thickness [mm]	0.48	0.65	0.88
apparent growth rate [μm/min]	32	37	154

[a] Tube diameters and number of walls were determined from HRTEM images (average of approximately 50 images per process). The areal density was estimated from the average diameter and weight of CNT carpets. The carpet thickness was determined from SEM images. The apparent growth rate was calculated as carpet thickness divided by duration of hydrogen exposure.

changes in the diameter and areal density of CNTs within the carpet, as well as in the average growth rate and final carpet thickness at the end of the process.

The curve in Figure 2 indicates the measured carpet height for varying times of hydrogen introduction for the process described above. This graph indicates that delaying hydrogen introduction leads to taller CNT carpets. However, not introducing hydrogen at all gives only micron-high carpets for the 15 min growth process.

The carpets that result from three specific processes (indicated by red dots in Figure 1) have been characterized in detail: H_2@−5, H_2@0, and H_2@+10. Figure 3 shows SEM images of the carpets obtained by introducing hydrogen before, at, and after ethylene introduction for the three selected processes. Delaying introduction of H_2 leads to better-aligned CNT carpets as well as taller carpets (therefore longer CNTs). HRTEM images (also shown in Figure 3) show that the CNT diameter and number of walls decreased, while the areal density increased, when hydrogen introduction was delayed. The average CNT diameter decreased from 14 nm (7 walls) for H_2@−5 to only 7 nm (3 walls) for H_2@+10. Concomitantly, the areal density increased by an order of magnitude from 4×10^9 CNTs/cm^2 for H_2@−5 to 5×10^{10} CNTs/cm^2 for H_2@+10 (refer to Table 1).

While CNT growth started almost instantly when H_2 and C_2H_4 were introduced simultaneously (approaching a steady growth rate within the first minute), exposure to C_2H_4 alone gave very slow growth. If we did not introduce hydrogen at all, after 15 min of exposure to C_2H_4 the carpet was only a few microns tall (Figure 4), from which we infer that most of the growth occurred when hydrogen is present. Although C_2H_4 indeed decomposes into hydrogen[37] (in addition to multiple carbon-based compounds), at our growth temperature (770 °C) we hypothesize that the C_2H_4 alone does not allow sufficient coarsening of the catalyst to affect CNT properties (the C_2H_4 flow rate is 150 sccm compared to the H_2 flow rate of 400 sccm). Furthermore, the formation of a carbide may dominate the growth phase in which only C_2H_4 is present (no added H_2).

We will define the "apparent growth rate" as equal to the carpet height divided by the hydrogen exposure time (Figure 5). When H_2 is introduced after the sample is exposed to C_2H_4 alone, the apparent growth rate increases rapidly. For example, introducing hydrogen 10 min after C_2H_4 gives an apparent growth rate of approximately 150 μm/minute, and the carpet attains a height of 0.88 mm after only five minutes of simultaneous exposure to C_2H_4 and H_2. This apparent growth rate is approximately five times the rate achieved when C_2H_4 and H_2 are introduced simultaneously. Furthermore, when hydrogen was introduced two minutes before the end of the process, we obtain a carpet of similar height as for H_2@+10, giving an apparent growth rate exceeding 400 μm/min (not shown).

AFM imaging of the as-deposited Fe/Al_2O_3 film (not shown) indicates a surface roughness below 0.25 nm, which does not change after heating to 770 °C in argon. AFM imaging of a sample without the Fe layer indicates a similar level of flatness (rms roughness below 0.25 nm), which is also retained after heating to 770 °C in argon or hydrogen (not shown).

To understand the effects of hydrogen on the catalyst, we annealed samples for increasing durations of hydrogen exposure at the growth temperature and then cooled rapidly to quench morphological evolution. This thermal process is illustrated in Figure 6. Note that these samples were cut from the same wafer we used for CNT growth and that no hydrocarbon gas was introduced during this thermal process. AFM measurements show that catalyst dots form after about 5 to 10 min, and that their height subsequently increases with longer times of exposure to hydrogen at 770 °C (Figure 7).

A full understanding of the CNT growth mechanism is complicated by the fact that iron can be present in many different oxidation states.[24] We will limit our analysis to the interpretation of the change in morphology and make selected assumptions regarding the oxidation state of the catalyst. Also, given that CNT lengths necessary for interconnect vias and for other electrical applications are in the submicron range, the thicknesses of the carpets studied here are more than sufficient for these applications.

Given the flatness of the as-deposited film, the small thickness (1.2 nm) of the deposited Fe catalyst layer and the pressure during deposition ($\sim 2 \times 10^{-6}$ Torr), we assume that the Fe catalyst layer is oxidized and continuous before starting the thermal process. On the basis of the Ellingham

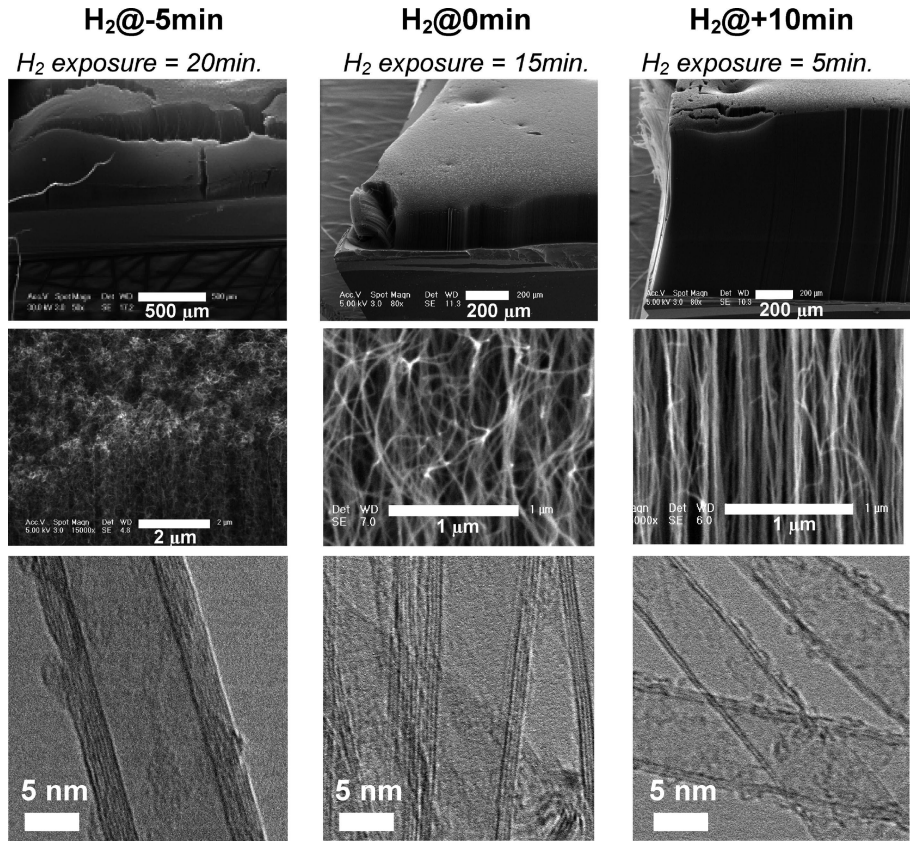

Figure 3. SEM and HRTEM images of CNT carpets after processing when H_2 is introduced 5 minutes before ethylene (H_2@−5), at the same time as ethylene (H_2@0), and 10 minutes after ethylene (H_2@+10). Delaying hydrogen introduction leads to taller CNT carpets, with better aligned CNTs, and with thinner CNTs with fewer walls.

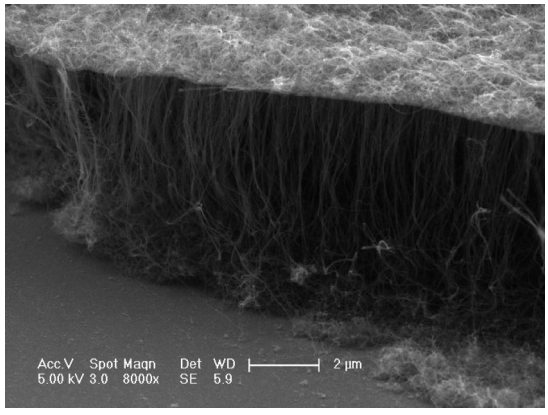

Figure 4. SEM image of CNTs grown for 15 min in C_2H_4/Ar only, without added hydrogen.

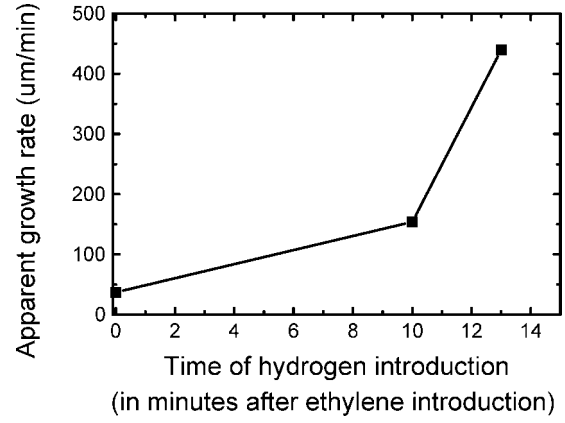

Figure 5. CNT apparent growth rate calculated as carpet height divided by hydrogen exposure time.

diagram[25] and the dynamics of oxidation of bulk iron,[26] we expect the starting oxide to be Fe_2O_3.[26] Because the argon used in these experiments contains a few parts per million of oxygen impurities, we can consider it an oxidizing atmosphere that, by keeping the catalyst layer oxidized, prevents dewetting of the catalyst.[18,27] Hence, a thermal process without hydrogen does not allow reduction of the iron oxide to iron, or the subsequent formation of catalyst clusters or particles. Once hydrogen is introduced, the iron oxide will be reduced and iron clusters will form. As observed by some teams using in situ XRD,[28] or in situ TEM,[29] or shown in molecular dynamics studies,[30] it is possible that, in between the oxide and the metal transformation, intermediate metastable carbide phases may be present after C_2H_4 is introduced.

The results shown in Figure 7 indicate that this process takes about 5−10 min at 770 °C. Using in situ XPS, Hofmann et al. observed that for Fe on SiO_2[31] and for Fe on Al_2O_3[27] the catalyst is active in its metallic state. Further, in an extensive study of the morphology and oxidation state of thin film Fe on alumina, Sushumna et al.[32] also observed that an Fe layer 12.5 Å thick is reduced to metallic iron when exposed to hydrogen at temperatures above 500 °C.

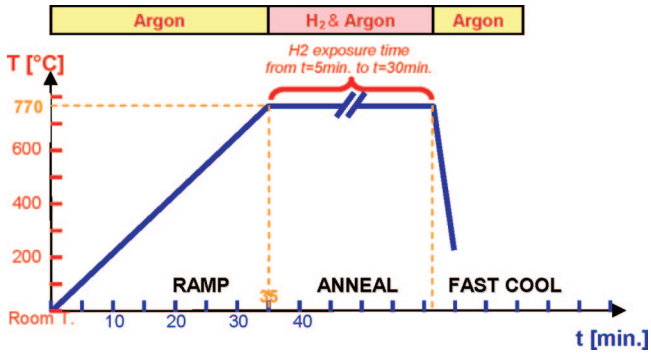

Figure 6. Thermal schedule for catalyst layers exposed only to H_2 and subsequently analyzed using an AFM. The only variable is the duration of hydrogen exposure.

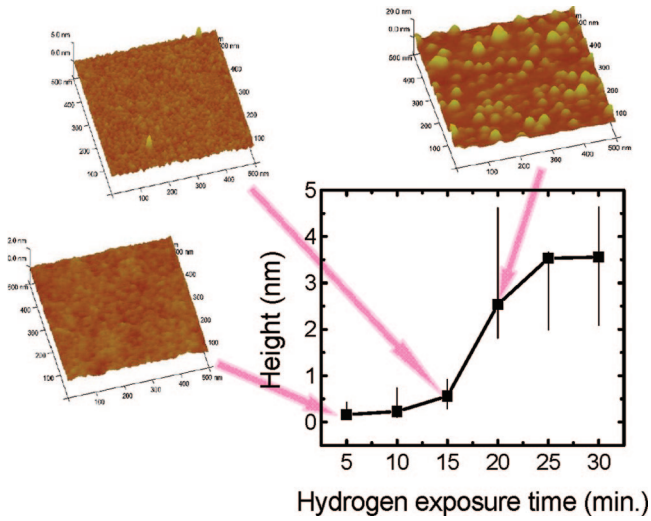

Figure 7. AFM images and catalyst height measurements as a function of time of exposure to H_2 at 770 °C. The catalyst layer dewets to form clusters and the cluster size (height) increases for longer exposure to hydrogen.

The clusters that form by film agglomeration after reduction of the iron oxide will initially be small, and consequently closely spaced. Continued annealing in the presence of H_2 allows the clusters to coarsen. This process, driven by surface energy minimization, occurs through transport of Fe among clusters, either through the vapor phase, or more likely by diffusion of Fe as adatoms on the Al_2O_3 surface. In coarsening processes, small clusters tend to shrink and disappear with their mass being redistributed to larger clusters. This process therefore results in an increase in the average cluster size as well as an increase in the average cluster spacing.[33,34] These trends are consistent with the observed trends in the average CNT diameter and areal density.

The curve shown in Figure 7 can therefore be interpreted as reflecting three regimes of behavior (as schematically illustrated in Figure 8):

(i) The initial rate of change is slow as hydrogen first reduces the catalyst layer.

(ii) Once the iron oxide is reduced, mobile iron adatoms form clusters.

(iii) The iron clusters coarsen at a rate that decreases with time.

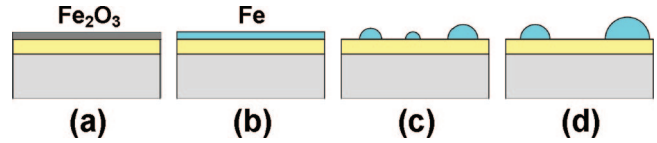

Figure 8. Schematic illustration of the evolution of the catalyst film with increased exposure to hydrogen. (a) The film is initially in the form of oxidized iron, (b) exposure to H_2 leads to reduction of the iron oxide, and (c) formation of Fe clusters or islands that (d) coarsen over time.

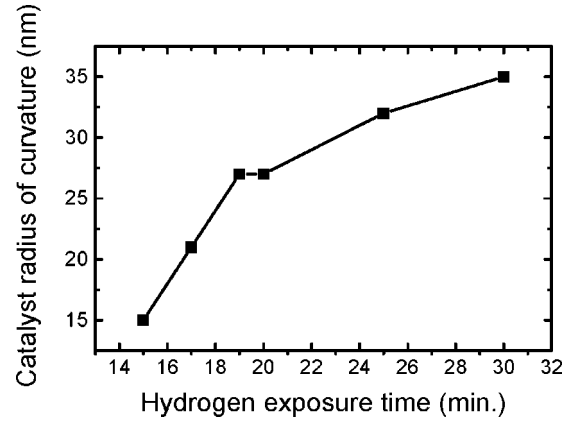

Figure 9. Average catalyst particle radius of curvature as a function of hydrogen exposure time, calculated from AFM line scans as described in the text.

Coarsening of the type observed in the last regime (Figure 7) is generally described by a function of the form

$$\langle r \rangle = Kt^n$$

where $\langle r \rangle$ is the average cluster size, K is a time-independent constant with a Boltzmann temperature dependence, t is time, and n is a constant (<1), the magnitude of which depends on the atomic mechanism that limits the rate of coarsening (e.g., adatom attachment to clusters or adatom diffusion on the substrate surface).[33,34] Evidence for catalyst coarsening after hydrogen annealing for iron deposited on SiO_2 has also been presented in an earlier study,[35] though no analysis of the process or its consequences were discussed.

We estimated the average radius of curvature of the catalyst dots from AFM images of samples subjected to various times of hydrogen exposure with the results shown in Figure 9. To determine the radius of the catalyst particles using AFM scans, we measured the particle height h as a function of position x for multiple horizontal scans of each AFM image and determined the radius of curvature about the particle apex, κ, using:

$$\kappa = \frac{h''(x)}{(1 + [h'(x)]^2)^{3/2}}$$

where the second and first derivatives of $h(x)$, $h'(x)$, and $h''(x)$, respectively, were determined numerically. This measure of $\langle r \rangle$, $1/\langle \kappa \rangle$, overestimates the true value of $\langle r \rangle$ but provides relative values of $\langle r \rangle$ that scale in the same way as their true values. As seen in Figure 9, we again find, as expected, that the initial coarsening rate is fast, but that the coarsening rate diminishes with time. Given that we expect the contact angle of the catalyst dots to remain the same,

independently of the time of exposure to hydrogen, the catalyst dot height and the radius of curvature should scale together.

As suggested earlier, the catalyst coarsening behavior observed without exposure of the catalysts to C_2H_4 correlates with the CNT characteristics as a function of the duration of pretreatment of the catalysts in H_2, indicating a mechanistic correlation. The similarity in trends can be illustrated by comparison of the average CNT diameter measured for the three process points in Figure 1 (13.6 nm for H_2@−5, 9.8 nm for H_2@0, and 7.4 nm for H_2@+10) and the three corresponding catalyst dot heights measured with AFM. These are 2.5 nm for H_2@−5 (corresponding to 5 min of H_2 exposure prior to the growth cycle and 15 min during the growth cycle), 0.6 nm for H_2@0 (corresponding to 15 min of H_2 exposure during the growth cycle), and 0.2 nm for H_2@+10 (corresponding to 5 min of H_2 exposure).

Owing to the accepted correlation between catalyst size and nanotube diameter,[36] we argue that the CNT diameter increases with increasing H_2 annealing time prior to introduction of C_2H_4 due to the increase in the average catalyst particle size that results from particle coarsening after exposure to H_2.

When H_2 and C_2H_4 are introduced simultaneously, the stages of reduction/coarsening and nucleation occur under the same reactant atmosphere. Here, the catalyst particles nucleate CNTs after sufficient reduction and clustering have occurred and before significant coarsening has occurred. Consequently, the CNTs have smaller diameters and are more closely spaced compared to when H_2 is introduced prior to C_2H_4.

When C_2H_4 is introduced before H_2, the catalyst experiences an extended period in which reduction and coarsening happen more slowly than when H_2 is added to the flow. Thermal decomposition of C_2H_4, which occurs as the gas is heated in the tube furnace and flows toward the sample, forms H_2 and a variety of additional hydrocarbons (e.g., CH_4, C_2H_6).[37] Therefore, a reducing environment is present when we introduce C_2H_4 without H_2. The presence of even smaller CNT diameters (relative to H_2@0) suggests that the coarsening kinetics in the atmosphere of C_2H_4 without added H_2 are slower than with C_2H_4/H_2 or H_2. Figures 2 and 5 also indicate that while H_2 reduction of iron oxide is required for growth, the shorter period of reduction results in the faster apparent rate of growth of CNTs. This implies that the rate of growth of CNTs from small iron clusters is much higher than rates implied for growth processes with longer H_2 exposure times. This may be the result of CNT etching during prolonged periods of exposure to H_2. The duration of exposure to H_2 therefore not only affects the CNT diameter and spacing through effects on the catalyst size, but also affects the apparent rate of CNT growth.

In summary, we have demonstrated that by controlling the time at which hydrogen is introduced during catalyzed thermal CVD of CNTs we can control the diameter, areal density, and apparent growth rate of CNTs (all three variables are coupled together). We have also shown that once the catalyst layer, initially oxidized iron, is reduced by exposure to H_2, clusters form and then coarsen over time. Introduction of hydrogen therefore leads not only to catalyst formation but also to catalyst coarsening. If CNT growth occurs immediately after reduction of the oxide, the catalysts are small and closely spaced, so that the catalyzed CNTs are also small and closely spaced. Furthermore, CNTs grown after only a brief exposure to H_2 have a very high apparent growth rate. This suggests that the extended presence of H_2 either leads to a slower growth rate or to etching of the CNTs after an initial rapid growth.

Acknowledgment. We would like to thank Nicola Abate for assistance with some of the experiments, Amanda Giermann, Dr. Ramkumar Krishnan, Dr. Reiner Moenig, Andrew Takahashi, Désirée Plata, and Dr. Kevin O'Brien (Intel), for useful discussions, and Libby Shaw for assistance with atomic force microscopy. This research was supported by the MARCO Interconnect Focus Center. G.D.N. was partially supported by an Intel Fellowship and A.J.H. was partially supported through a Fannie and John Hertz Foundation Fellowship.

References

(1) Dresselhaus, M. S.; Dresselhaus, G.; Avouris, P. *Carbon Nanotubes: Synthesis, Structure, Properties, and Applications*; Springer: Berlin, 2001.
(2) Baughman, R. H.; Zakhidov, A. A.; de Heer, W. A. *Science* **2002**, *297* (5582), 787–792.
(3) Nihei, M.; Kawabata, A.; Kondo, D.; Horibe, M.; Sato, S.; Awano, Y. *Jpn. J. Appl. Phys.* **2005**, *44* (4A), 1626–1628.
(4) Tong, T.; Zhao, Y.; Delzeit, L.; Kashani, A.; Meyyappan, M.; Majumdar, A. *IEEE Trans. Compon., Packag. Technol.* **2007**, *30* (1), 92–100.
(5) García, E. J.; Wardle, B. L.; Hart, A. J. Joining Prepreg Composite Interfaces with Aligned Carbon Nanotubes. *Composites, Part A* **2008**, *39* (6), 1065–1070.
(6) Naeemi, A.; Meindl, J. D. *IEE Trans. Electron Devices* **2007**, *54* (1), 26–37.
(7) Awano, Y.; Sato, S.; Kondo, D.; Ohfuti, M.; Kawabata, A.; Nihei, M.; Yokoyama, N. *Phys. Status Solidi A* **2006**, *203* (14), 3611–3616.
(8) Li, H. J.; Lu, W. G.; Li, J. J.; Bai, X. D.; Gu, C. Z. *Phys. Rev. Lett.* **2005**, *95* (8),
(9) Delzeit, L.; Nguyen, C. V.; Chen, B.; Stevens, R.; Cassell, A.; Han, J.; Meyyappan, M. *J. Phys. Chem. B* **2002**, *106* (22), 5629–5635.
(10) Fan, S. S.; Chapline, M. G.; Franklin, N. R.; Tombler, T. W.; Cassell, A. M.; Dai, H. J. *Science* **1999**, *283* (5401), 512–514.
(11) Hart, A. J.; Slocum, A. H. *J. Phys. Chem. B* **2006**, *110*, 8250–8257.
(12) Hata, K.; Futaba, D. N.; Mizuno, K.; Namai, T.; Yumura, M.; Iijima, S. *Science* **2004**, *306* (5700), 1362–1364.
(13) Li, Y. M.; Kim, W.; Zhang, Y. G.; Rolandi, M.; Wang, D. W.; Dai, H. J. *J. Phys. Chem. B* **2001**, *105* (46), 11424–11431.
(14) Chakrabarti, S.; Kume, H.; Pan, L. J.; Nagasaka, T.; Nakayama, Y. *J. Phys. Chem. C* **2007**, *111* (5), 1929–1934.
(15) Hofmann, S.; Cantoro, M.; Kleinsorge, B.; Casiraghi, C.; Parvez, A.; Robertson, J.; Ducati, C. *J. Appl. Phys.* **2005**, *98* (3), 34308–1.
(16) Yamada, T.; Namai, T.; Hata, K.; Futaba, D. N.; Mizuno, K.; Fan, J.; Yudasaka, M.; Yumura, M.; Iijima, S. *Nat. Nanotechnol.* **2006**, *1* (2), 131–136.
(17) Cantoro, M.; Hofmann, S.; Pisana, S.; Ducati, C.; Parvez, A.; Ferrari, A. C.; Robertson, J. *Diamond Relat. Mater.* **2006**, *15* (4−8), 1029–1035.
(18) Cantoro, M.; Hofmann, S.; Pisana, S.; Scardaci, V.; Parvez, A.; Ducati, C.; Ferrari, A. C.; Blackburn, A. M.; Wang, K. Y.; Robertson, J. *Nano Lett.* **2006**, *6* (6), 1107–1112.
(19) Bennett, R. D.; Hart, A. J.; Cohen, R. E. *Adv. Mater.* **2006**, *18*, 2274–2279.
(20) Nishiyama, Y.; Tamai, Y. *J. Catal.* **1976**, *45* (1), 1–5.
(21) Zhang, G.; Mann, D.; Zhang, L.; Javey, A.; Li, Y.; Yenilmez, E.; Wang, Q.; McVittie, J. P.; Nishi, Y.; Gibbons, J.; Dai, H. *Proc. Natl. Acad. Sci. U.S.A.* **2005**, *102* (45), 16141–16145.
(22) Futaba, D. N.; Hata, K.; Yamada, T.; Mizuno, K.; Yumura, M.; Iijima, S. *Phys. Rev. Lett.* **2005**, *95*, 056104.

(23) Futaba, D. N.; Hata, K.; Namai, T.; Yamada, T.; Mizuno, K.; Hayamizu, Y.; Yumura, M.; Iijima, S. *J. Phys. Chem. B* **2006**, *110* (15), 8035–8038.
(24) Cornell, R. M.; Schwertmann, U. *The iron oxides: structure, properties, reactions, occurrences, and uses*, 2nd ed.; Wiley-VCH: Weinheim, 2003; p 11.
(25) Gaskell, D. R. *Introduction to the thermodynamics of materials*, 4th ed.; Taylor & Francis: New York, 2003; p 359.
(26) Bertrand, N.; Desgranges, C.; Gauvain, D.; Monceau, D.; Poquillon, D. High Temperature Corrosion and Protection of Materials 6, Prt 1 and 2, Proceedings *Mater. Sci. Forum* **2004**, *461−464*, 591−598.
(27) Hofmann, S. In *Interface Dynamics of Crystalline Catalysts during Carbon Nanotube Growth*; Materials Research Society Fall Conference, November 26, 2007, Boston, MA. Unpublished work, 2007.
(28) Nishimura, K.; Okazaki, N.; Pan, L. J.; Nakayama, Y. *Jpn. J. Appl. Phys., Part 2* **2004**, *43* (4A), L471−L474.
(29) Schaper, A. K.; Hou, H. Q.; Greiner, A.; Phillipp, F. *J. Catal.* **2004**, *222* (1), 250–254.
(30) Ding, F.; Bolton, K.; Rosen, A. *J. Phys. Chem. B* **2004**, *108* (45), 17369–17377.
(31) Hofmann, S.; Sharma, R.; Ducati, C.; Du, G.; Mattevi, C.; Cepek, C.; Cantoro, M.; Pisana, S.; Parvez, A.; Cervantes-Sodi, F.; Ferrari, A. C.; Dunin-Borkowski, R.; Lizzit, S.; Petaccia, L.; Goldoni, A.; Robertson, J. *Nano Lett.* **2007**, *7* (3), 602–608.
(32) Sushumna, I.; Ruckenstein, E. *J. Catal.* **1985**, *94* (1), 239–288.
(33) Chakraverty, B. K. *J. Phys. Chem. Solids* **1967**, *28* (12), 2401–2412.
(34) Thompson, C. V. *Acta Metall.* **1988**, *36* (11), 2929–2934.
(35) Pisana, S.; Cantoro, M.; Parvez, A.; Hofmann, S.; Ferrari, A. C.; Robertson, J. *Physica E* **2007**, *37* (1−2), 1–5.
(36) Chhowalla, M.; Teo, K. B. K.; Ducati, C.; Rupesinghe, N. L.; Amaratunga, G. A. J.; Ferrari, A. C.; Roy, D.; Robertson, J.; Milne, W. I. *J. Appl. Phys.* **2001**, *90* (10), 5308–5317.
(37) Gordon, D.; Towell, J. J. M. *AIChE J.* **1961**, *7* (4), 693–698.

NL801437C